



Microwave coplanar band-stop filters based on electric-LC resonators: systematic numerical approach and experimental validation

Martino Aldrigo¹ · Leonardo Zappelli² · Alina Cismaru¹ · Mircea Dragoman¹ · Sergiu Iordanescu¹ · Damir Mladenovic¹ · Catalin Parvulescu¹ · Hardly C. Joseph² · Davide Mencarelli² · Luca Pierantoni² · Paola Russo²

Received: 10 November 2022 / Accepted: 17 April 2023
© The Author(s) 2023

Abstract

In this paper, we propose a comparative method to analyze a complex microwave structure consisting of a silicon-based coplanar waveguide line and four electric-LC resonators, thus forming a wideband microwave band-stop filter that can be easily integrated at the wafer level together with other devices and sub-systems for large-scale production of high-frequency electronics. A rigorous and careful approach is needed when choosing the proper simulation settings and, as a good rule of thumb, both time and frequency domains should provide the same results. Furthermore, the experimental validation requires supplementary components (like connectors), often ignored when designing an electromagnetic structure highly impacting on the overall performance. In this work, we go in depth into all these issues and show how the right choices in terms of computational parameters can lead to a good agreement with the measurements of the proposed CMOS-compatible band-stop filter in the band 2–18 GHz, with a relative bandwidth of almost 30% around the band-stop frequency of 13.2 GHz and a rejection level of –40 dB.

Keywords Coplanar waveguide · Microwave filters · Planar resonators

1 Introduction

Many papers have investigated the propagation of the electromagnetic (EM) fields in coplanar waveguides (CPW) or in striplines loaded with metamaterial-based resonators, such as split-ring resonators (SRRs) [1–3] or electric-LC resonators (ELCRs) [4, 5], for applications in filters [6–8], antennas [9, 10], or in energy harvesting [5]. The resonators can

be placed either in the same plane of the CPW [7] or in the back side of the substrate [1–3]. Irrespective of the resonator placement, the electromagnetic analysis of the structure is very complex for any kind of application and it is usually carried out by means of numerical techniques using an electromagnetic simulation tool, such as HFSS or CST Microwave Studio, or other semi-analytical approaches [11]. At a first glance, the numerical analysis could appear a simple

✉ Leonardo Zappelli
l.zappelli@univpm.it

Martino Aldrigo
martino.aldrigo@imt.ro

Alina Cismaru
alina.cismaru@imt.ro

Mircea Dragoman
mircea.dragoman@imt.ro

Sergiu Iordanescu
sergiu.iordanescu@imt.ro

Damir Mladenovic
damir.mladenovic@imt.ro

Catalin Parvulescu
catalin.parvulescu@imt.ro

Hardly C. Joseph
h.j.christopher@univpm.it

Davide Mencarelli
d.mencarelli@univpm.it

Luca Pierantoni
l.pierantoni@univpm.it

Paola Russo
p.russo@univpm.it

¹ IMT-Bucharest, 077190 Voluntari, Ilfov, Romania

² Dipartimento di Ingegneria dell'Informazione, Università Politecnica delle Marche, 60131 Ancona, Italy

task thanks to the computational capabilities of commercial EM simulators; however, there are some artifices that should be used to obtain reliable outputs to be compared with the experimental results. On the other hand, the complete measurement setup (i.e., comprehensive of connectors, probe tips, dielectric/metallic support, etc.) should be included in the EM design as well, to represent the real scenario in which the designed structure will be characterized.

The aim of this paper is to propose a rigorous and exhaustive analysis of how to properly simulate (using CST Microwave Studio) a silicon-based CPW line loaded with in-plane ELCRs (Fig. 1a) and realized with the multilayer structure shown in Fig. 1b (with $t_{Si} = 525 \mu\text{m}$ (high-resistivity silicon or HRSi) and $t_{gold} = t_{SiO_2} = 500\text{nm}$), which offers CMOS compatibility and ease of integration together with other devices and components. The integration with the devices/components is a highly desirable target for high-frequency electronics, together with its CMOS compatibility, and it is one of the advantages of the presented filter in comparison with the actual state of the art, as it will be summarized in the last table of this paper. We will present the optimal choice of simulation and modeling settings to optimize the computational effort (e.g., number of mesh cells, type and dimensions of excitation ports, etc.) both in the frequency (FD) and time (TD) domain, and the obtained results will be compared with the experimental ones, showing an excellent

agreement. One of the most important questions is: Which is the best domain (i.e., FD or TD) to simulate the device under test (DUT)? As expected, there is no definitive answer, even if CST suggests the use of one or the other domain, depending on the complexity of the DUT itself. In some cases, both domains could offer similar results, hence leaving doubt over which method is the most reliable and the fastest. In this case, a direct comparison between the FD and TD can be useful to understand the correctness of the simulation outputs. The paper will also investigate the choice of (i) the most appropriate waveguide ports for the stimulation and evaluation of the scattering (S) parameters, (ii) the mesh, and (iii) the strategy to select the frequency points to optimize the adaptive mesh.

2 Numerical simulations

The analyzed structure is characterized by $w_{line} = 0.3$, $w_{gap} = 0.19$, $w_{ring} = 1.55$, $g = 0.15$, $w_{taper} = 2.15$, $w_{bot} = 7.274$, $t_{ring} = 0.15$, $\delta = 0.125$, $L_{channel} = 8.6$, $L_{taper} = 0.85$, and $d = 2.85$ (all dimensions in mm), whereas the band of interest is 2–18 GHz (S, C, X, and Ku bands). This was a requirement in the frame of a project for which a band-stop filter integrating ELCRs was necessary. Hence, the specific design chosen and the filter realization aimed at fulfilling project's specifications: This led to a thorough investigation of the filter modeling from an electromagnetic point of view. The first problem to be tackled is the proper choice of the ports for the excitation of the DUT and the evaluation of the S parameters. For this kind of open structures, we chose the “waveguide ports” with a magnetic symmetry wall in the longitudinal plane $y - z$, whereas the boundary conditions for the transverse plane $x - y$ are “open (add space).”

2.1 Port settings

The choice of the dimensions of the waveguide ports is an important key to obtain reliable results (i.e., with a physical meaning and in agreement with the experiments). Referring to Fig. 1b, the waveguide port dimensions w_{port} and t_{port} should enclose completely the propagating EM field. While for a closed waveguide the previous condition is attained by setting the port dimensions equal to the cross section of the input and output waveguides, for open planar structures the choice is far more complex, since the port cross section should contain almost entirely the EM field (i.e., quasi-TEM mode in the present case of study). The used software suggests to apply a port width $w_{port} = n_{w_p} (w_{line} + 2w_{gap})$ with $3 \leq n_{w_p} \leq 5$, whereas the height should extend on the top air and in the bulk substrate; however, a range for the variation of t_{port} is not

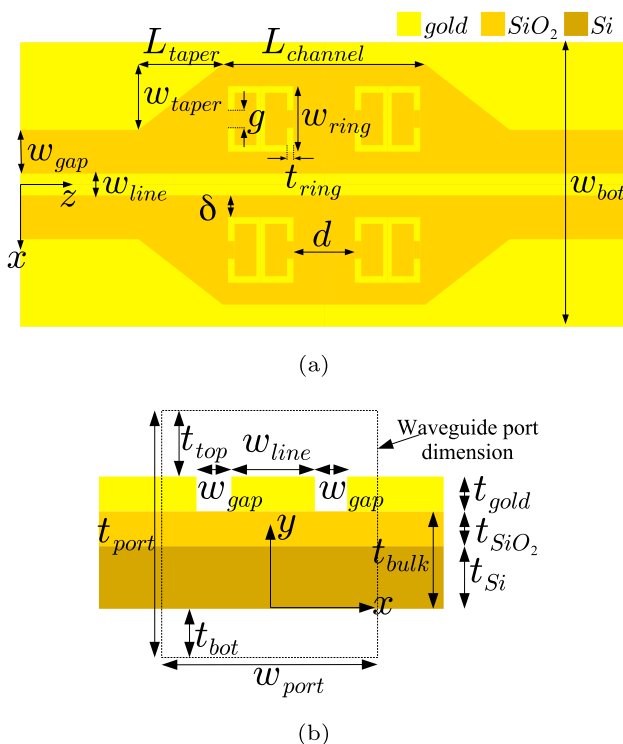


Fig. 1 Geometry of the CPW line with in-plane ELCRs (not in scale): **a** longitudinal section; **b** cross section

clearly defined. Moreover, the port dimensions should be not too large to avoid the excitation of spurious higher-order modes. The best solution is to choose w_{port} and t_{port} by simulating a simple straight CPW line with the same cross section of the actual structure at the port sections and then to analyze the behavior of the obtained S parameters. For the straight lossy CPW line, we have $S_{11} = 0$ and $S_{21} = e^{-(\alpha+j\beta)L_{\text{CPW}}}$, where $\alpha + j\beta$ is the complex propagation constant. In a numerical simulation, the dimensions of the waveguide ports can be chosen to satisfy the previous values for S_{11} and S_{21} with a reasonable, pre-defined accuracy. For the CPW used in this work, we report $|S_{11}|$ and $|S_{21}|$ in Fig. 2 by varying the dimensions of the waveguide ports, setting (i) $w_{\text{port}} = n_{w_p}(w_{\text{line}} + 2w_{\text{gap}})$ for the side extension of the ports and (ii) $t_{\text{top}} = n_{\text{top}}t_{\text{bulk}}$ and $t_{\text{bot}} = n_{\text{bot}}t_{\text{bulk}}$ for the vertical extension, with $n_{w_p} = 3, 4, 5$, $n_{\text{top}} = 1, 1.5, 2$, and $n_{\text{bot}} = -0.5, 1, 1.5$.

$|S_{11}|$ shows poor values for the $n_{\text{bot}} = -0.5$ family set for any value of n_{w_p} and n_{top} , as highlighted by the red lines in Fig. 2. This is due to the fact that the port includes only half of the bulk substrate, thus neglecting a significant amount of EM field. Setting $n_{\text{bot}} \geq 1$, the results become much more reliable. As expected, the extension of the port in the top and side parts lowers $|S_{11}|$ as well, as shown by the dashed black, solid blue, and solid green lines for $|S_{11}|$ in Fig. 2. The lines with symbols refer to $|S_{11}|$ for $n_{\text{bot}} = 1.5$, $n_{\text{top}} = 2$, and $n_{w_p} = 3$ (black), 4 (blue), 5 (green). The presence of multiple minima is due to the finite dimensions of the simulated ports, which entails a power reflection from the area not covered by the receiving port at the opposite side. This reflection reduces by increasing the port dimensions.

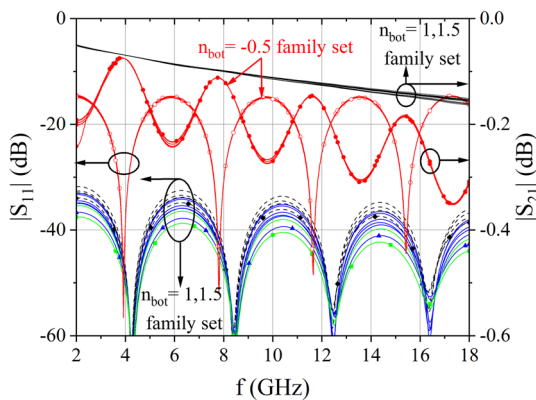


Fig. 2 $|S_{11}|$ and $|S_{21}|$ for a straight CPW line by varying the dimensions of the waveguide ports with n_{w_p} , n_{top} , and n_{bot} . The red lines refer to the $n_{\text{bot}} = -0.5$ family set; the solid black lines refer to $|S_{21}|$ for any family set; and the dashed black, solid blue, and solid green lines refer to $|S_{11}|$ ($n_{w_p} = 3, 4, 5$ and $n_{\text{top}} = 1, 1.5, 2$ for $n_{\text{bot}} = 1, 1.5$ family sets) (Color figure online)

2.1.1 Taper analysis

Once the port dimensions have been set, the analysis of the tapers in the CPW line must be addressed to verify their influence upon the S parameters. Moreover, it is important to understand the differences between the numerical results for the FD and TD to choose the best domain in terms of run time, memory occupation, and convergence. The differences between FD (tetrahedral mesh) and TD (hexahedral mesh) results are less than 0.5 dB up to 16 GHz and increase in the remaining part of the considered band, whereas the minima are very similar (Fig. 3). The maximum number of mesh cells per wavelength was set to 35 for both domains, but the adaptive mesh refinement ($\Delta S_{ij} < 0.01$ at two consecutive adaptive mesh steps) produces different final values: The convergence was obtained with about 2.5 M cells for the TD and with about 0.4 M cells for the FD, whereas the run time was about the same (1 h 15 m). It should be recalled that the adaptive mesh procedure is different in the two domains. Moreover, while the direct comparison between the number of cells in the two domains gives a benchmark on the correct discretization of the DUT, the comparison between the memory usage for the two domains is also important. It should be recalled that tetrahedral (FD) and hexahedral (TD) mesh types require a different memory usage. Hence, for this particular structure the comparison between correct discretization, memory usage, and run time suggests that the choice of the FD could be the best one.

2.1.2 ELCR analysis

The last simulation is the global, complex structure shown in Fig. 1a (embedding the 4 ELCRs), and the corresponding S parameters are shown in Fig. 4b in comparison with the measurements performed on the fabricated DUT (Fig. 4a). The TD and FD simulations are displayed with blue (FD)

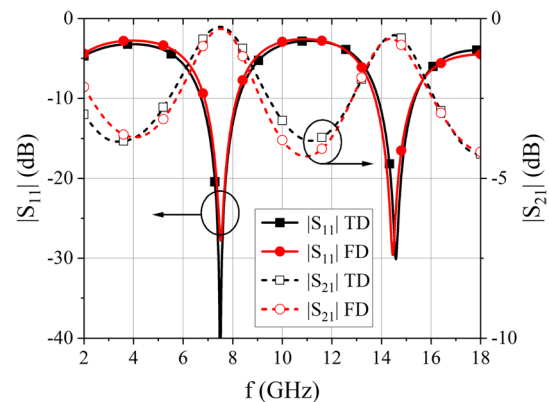


Fig. 3 ($|S_{11}|$ (left axis) and $|S_{21}|$ (right axis) for the CPW line with tapers evaluated with the time (TD: black lines) and frequency (FD: red lines) domain (Color figure online)

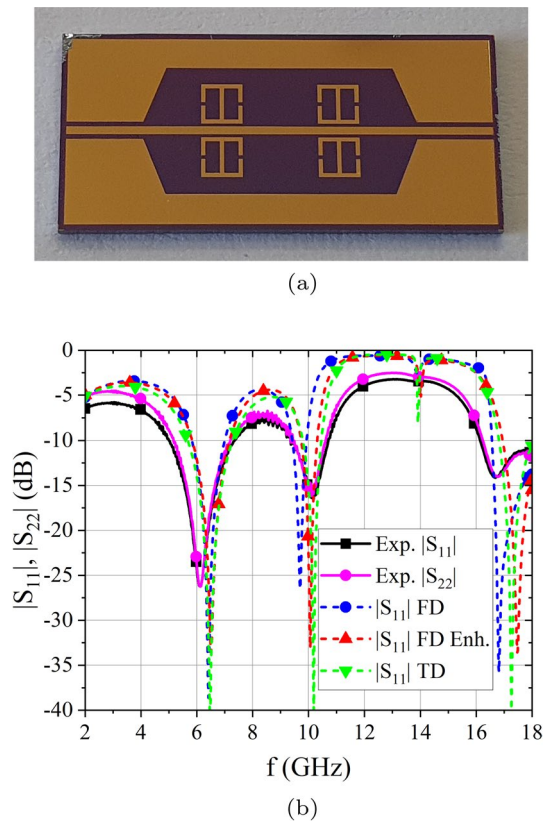


Fig. 4 **a** Optical picture of the CPW line loaded with 4 ELCRs; **b** comparison between numerical (dashed lines) and experimental (continuous lines) results for CPW with ELCRs

and green (TD) lines, and there are some differences in the position of the $|S_{11}|$ minima ($|S_{11}| = |S_{22}|$) for numerical simulations). This is due to the differences in the mesh (2 M for the TD vs 0.18 M for the FD) obtained by the two methods starting from the same number of mesh cells per wavelength.

The FD results can be improved by adding in the simulations auxiliary frequency points where the adaptive mesh must be evaluated. This can be done setting (a) a maximum number of points automatically chosen by the FD solver or (b) choosing single frequency points where the numerical evaluation must be improved. The first choice produces a very accurate adaptive evaluation of the S parameters at many points, but at the expense of a very large number of mesh cells that can grow without any control. On the contrary, the second choice produces an accurate adaptive evaluation only at the selected frequency points but with a lower computational effort in terms of mesh cells. Hence, if the single frequency points are carefully chosen, the global evaluation of the S parameters can be enhanced with a limited number of mesh cells.

We opted in favor of the second strategy even if it is not simple to choose “*a priori*” the better placement of the auxiliary frequency points. One choice could be a uniform

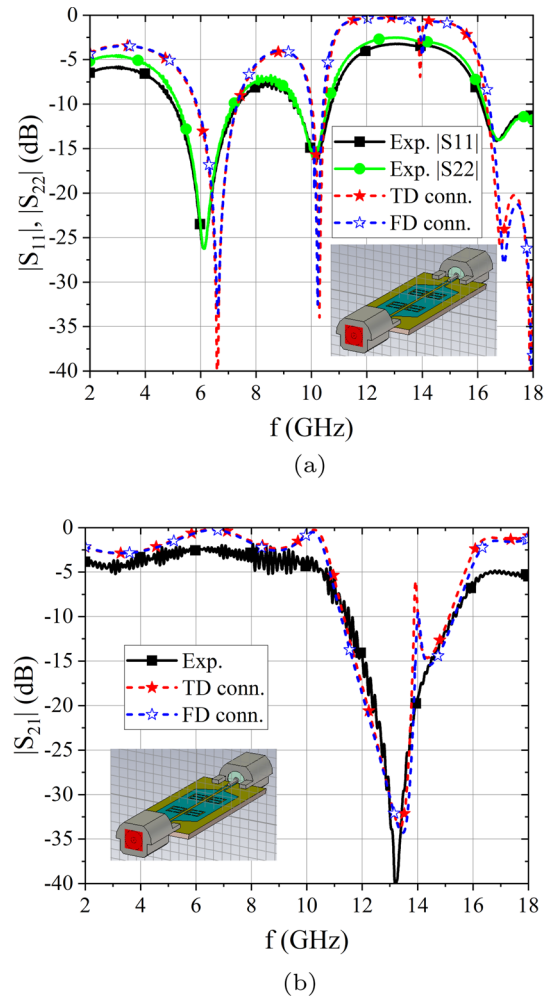


Fig. 5 **a–b** Comparison between numerical (dashed lines) and experimental (continuous lines) results for CPW loaded with ELCRs and fed by SMPM connectors

distribution over the frequency band, or to put them in correspondence of maxima or/and minima of $|S_{11}|$. In our case, we added in the simulations two frequency points corresponding to the position of the two $|S_{11}|$ minima (i.e., at 6 and 10 GHz). The global number of mesh cells in the FD increases to 0.5 M, and the results become very similar for both TD and FD, as shown by the red lines labeled with “FD Enh.” in Fig. 4b. It should be stressed that the enhanced FD requires a longer run time than that of the TD and also needs a high memory usage. The overall behavior of the measured reflection coefficients (solid lines in Fig. 4b) is also in good agreement with the simulations, apart from lower values in the experimental $|S_{11}|$ and $|S_{22}|$, which is likely due to supplementary losses. Nevertheless, the two minima at 6 and 10 GHz are well reproduced, whereas the little difference between the measured values of $|S_{11}|$ and $|S_{22}|$ is probably due to slight misalignments of the connectors at the two ports. The uncertainty about the port dimensions can be further

Table 1 Simulation details of the proposed ELCR-based band-stop filter

Type of feeding technique	Frequency Domain (FD)						Time Domain (TD)		
	Mesh Cells (Millions)		Run Time (Hours)		Memory (GB)		Mesh Cells (Millions)	Run Time (Hours)	Memory (GB)
Wave port	Auto	Enh	Auto	Enh	Auto	Enh	2.04	0.3	0.45
	0.18	0.5	0.27	0.87	15	28			
SMPM Connector	n.a.	0.4	n.a.	0.92	n.a.	26	4.2	2.5	0.75

reduced by adding an SMPM connector in the CST simulations to simulate the correct excitation of the CPW structure, as it is shown in the inset of Fig. 5a. We have reproduced an SMPM connector in CST by public technical outline drawings found on the Internet. The numerical simulations shown in Fig. 5a–b are in good agreement with the experimental results for both FD (enhanced type) and TD. The differences in the amplitude of the *S* parameters are likely due to some loss mechanisms that cannot be easily taken into account in the simulations, e.g., connectors-metallization contact resistance, potential microscale misalignments between the tips of the connectors and the CPW, and chemical residuals after metal deposition. This can be confirmed by the power loss shown in Fig. 6: The loss behavior vs frequency is similar,

but the entity is much greater in the experimental results. The global overview of the performance of the FD and TD simulation approaches in terms of computational effort (i.e., number of mesh cells, run time, and memory usage), for different types of feeding techniques, is presented in Table 1.

Finally, Table 2 offers a comprehensive comparison among different band-stop filters embedding metamaterials and planar transmission lines. The considered filters mostly used complementary split-ring resonators (CSRRs) or SRRs in microstrip technology. The filter proposed in this work operates at a much higher frequency and provides a wider bandwidth (calculated at the reference level of -10 dB). Moreover, the rejection level is greatly improved with respect to the actual state of the art. Another significant advantage is represented by the CMOS compatibility characteristics of the presented solution (whereas the other ones are all fabricated using PCB technology): This approach facilitates the integration at the wafer level of such components together with other devices and sub-systems for large-scale production of high-frequency electronics.

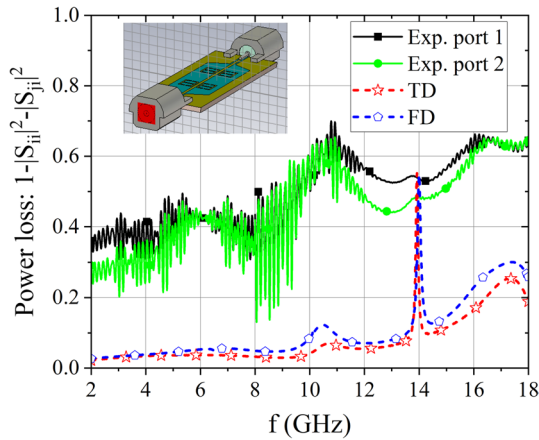


Fig. 6 Evaluation of the power loss for numerical and experimental results

3 Conclusion

In this paper, we have presented a comprehensive treatment about the rigorous electromagnetic simulations, in both time and frequency domain, of a CMOS-compatible microwave band-stop filter based on a coplanar waveguide integrated with four electric-LC resonators. To tackle the problems arising from unavoidable numerical approximations needed to simulate the wideband properties of such

Table 2 Comparison of metamaterial-based band-stop filters

Ref.	Type of metamaterials	Configuration	Center frequency (GHz)	Bandwidth* (GHz)	Rejection level (dB)	Technology
[12]	CSRR	Microstrip	5.4	0.8 (14.8%)	- 22	PCB
[13]	CSRR	Microstrip	2	0.4 (20%)	- 28	PCB
[14]	SRR	Coplanar waveguide	7.7	0.25 (3.2%)	- 25	PCB
[15]	SRR	Microstrip	1.90	0.13 (6.8%)	- 25	PCB
This work	Electric-LC	Coplanar waveguide	13.2	3.9 (29.5%)	- 40	CMOS

*Ref. level: - 10 dB

complex structures, we have taken into account the most important computational settings, like port dimensions and choice of the frequency adaptive mesh points, to obtain reliable simulation results. Moreover, in order to well reproduce the measurement setup, we have carried out an exhaustive investigation on the effect of external components affecting the ideal situation, like connectors. The output is in good agreement with the experimental characterization. The performed analysis is of great importance for any electromagnetic design and can be applied in a straightforward way to any task involving complicated microwave structures.

Author contributions All authors contributed to the study conception and design. Material preparation, data collection, and analysis were performed by MA, LZ, and AC. The first draft of the manuscript was written by MA and LZ, and all authors commented on previous versions of the manuscript. All authors read and approved the final manuscript.

Funding Open access funding provided by Università Politecnica delle Marche within the CRUI-CARE Agreement. This research was supported by the European Project H2020 FETOPEN-01-2018-2019-2020 "NANOPOLY" under Grant No. 829061 and by the Romanian Core Program within the National Research Development and Innovation Plan 2022–2027, carried out with the support of MCID, Project No. 2307.

Data availability The datasets generated during and/or analyzed during the current study are not publicly available due to Intellectual Property reasons but are available from the corresponding author on reasonable request.

Declarations

Conflict of interest The authors have no relevant financial or non-financial interests to disclose.

Open Access This article is licensed under a Creative Commons Attribution 4.0 International License, which permits use, sharing, adaptation, distribution and reproduction in any medium or format, as long as you give appropriate credit to the original author(s) and the source, provide a link to the Creative Commons licence, and indicate if changes were made. The images or other third party material in this article are included in the article's Creative Commons licence, unless indicated otherwise in a credit line to the material. If material is not included in the article's Creative Commons licence and your intended use is not permitted by statutory regulation or exceeds the permitted use, you will need to obtain permission directly from the copyright holder. To view a copy of this licence, visit <http://creativecommons.org/licenses/by/4.0/>.

References

1. Sanz, V., Belenguer, A., Martinez, L., Borja, A.L., Cascon, J., Boria, V.E.: Balanced right/left-handed coplanar waveguide with stub-loaded split-ring resonators. *IEEE Antennas Wirel. Propag. Lett.* **13**, 193–196 (2014)
2. Elsheikh, M.A.G., Ammar, N.Y., Safwat, A.M.E.: Analysis and design guidelines for wideband CRLH SRR-loaded coplanar waveguide. *IEEE Trans. Microw. Theory Tech.* **68**(7), 2562–2570 (2020)
3. Naqui, J., Duran-Sindreu, M., Martin, F.: Modeling split-ring resonator (SRR) and complementary split-ring resonator (CSRR) loaded transmission lines exhibiting cross-polarization effects. *IEEE Antennas Wirel. Propag. Lett.* **12**, 178–181 (2013)
4. Ghaderi, B., Nayyeri, V., Soleimani, M., Ramahi, O.M.: A novel symmetric ELC resonator for polarization-independent and highly efficient electromagnetic energy harvesting. In: *IEEE IMWS-AMP*, pp. 1–3 (2017)
5. Withayachumnankul, W., Fumeaux, C., Abbott, D.: Planar array of electric-LC resonators with broadband tunability. *IEEE Antennas Wirel. Propag. Lett.* **10**, 577–580 (2011)
6. Horestani, A.K., Duran-Sindreu, M., Naqui, J., Fumeaux, C., Martin, F.: Coplanar waveguides loaded with s-shaped split-ring resonators: modeling and application to compact microwave filters. *IEEE Antennas Wirel. Propag. Lett.* **13**, 1349–1352 (2014)
7. Ponchak, G.E.: Coplanar stripline coupled to planar double split-ring resonators for bandstop filters. *IEEE Microw. Wirel. Compon. Lett.* **28**(12), 1101–1103 (2018)
8. Martin, F., Falcone, F., Bonache, J., Marques, R., Sorolla, M.: Miniaturized coplanar waveguide stop band filters based on multiple tuned split ring resonators. *IEEE Microw. Wirel. Compon. Lett.* **13**(12), 511–513 (2003)
9. Siddiqui, J.Y., Saha, C., Antar, Y.M.M.: Compact dual-SRR-loaded UWB monopole antenna with dual frequency and wide-band notch characteristics. *IEEE Antennas Wirel. Propag. Lett.* **14**, 100–103 (2015)
10. Li, M., Lin, X.Q., Chin, J.Y., Liu, R., Cui, T.J.: A novel miniaturized printed planar antenna using split-ring resonator. *IEEE Antennas Wirel. Propag. Lett.* **7**, 629–631 (2008)
11. Chen, Z., Wang, C.F., Hoefer, W.J.R.: A unified view of computational electromagnetics. *IEEE Trans. Microw. Theory Tech.* **70**(2), 955–969 (2022)
12. Ali, A., Hu, Z.: Metamaterial resonator based wave propagation notch for ultrawideband filter applications. *IEEE Antennas Wirel. Propag. Lett.* **7**, 210–212 (2008)
13. Ebrahimi, A., Withayachumnankul, W., Al-Sarawi, S.F., Abbott, D.: Compact second-order bandstop filter based on dual-mode complementary split-ring resonator. *IEEE Microw. Wirel. Compon. Lett.* **26**(8), 511–513 (2016)
14. Kim, J., Cho, C.S., Lee, J.W.: Cpw bandstop filter using slot-type srrs. *Electron. Lett.* **41**, 1333–1334 (2005)
15. Yan, L., Tang, M., Krozer, V., Zhurbenko, V., Jiang, C., Johansen, T.K.: Filter designs based on coupled transmission line model for double split ring resonators. *Microw. Opt. Technol. Lett.* **54**(2), 467–471 (2012)

Publisher's Note Springer Nature remains neutral with regard to jurisdictional claims in published maps and institutional affiliations.